

# Strong IMF By-related plasma convection in the ionosphere and cusp field-aligned currents under northward IMF conditions

G. Le<sup>1</sup>, G. Lu<sup>2</sup>, R. J. Strangeway<sup>3</sup>, R. F. Pfaff, Jr.<sup>1</sup>

<sup>1</sup> Laboratory for Extraterrestrial Physics, NASA Goddard Space Flight Center, Greenbelt, MD

<sup>2</sup> High Altitude Observatory, NCAR, Boulder, CO

<sup>3</sup> Institute of Geophysics and Planetary Physics, University of California, Los Angeles, CA

## Abstract.

We present in this paper an investigation of IMF-By related plasma convection and cusp field-aligned currents using FAST data and AMIE model during a prolonged interval with large positive IMF By and northward Bz conditions ( $B_y/B_z \gg 1$ ). Using the FAST single trajectory observations to validate the global convection patterns at key times and key locations, we have demonstrated that the AMIE procedure provides a reasonably good description of plasma circulations in the ionosphere during this interval. Our results show that the plasma convection in the ionosphere is consistent with the anti-parallel merging model. When the IMF has a strongly positive  $B_y$  component under northward conditions, we find that the global plasma convection forms two cells oriented nearly along the Sun-earth line in the ionosphere. In the northern hemisphere, the dayside cell has clockwise convection mainly circulating within the polar cap on open field lines. A second cell with counterclockwise convection is located in the nightside circulating across the polar cap boundary. The observed two-cell convection pattern appears to be driven by the reconnection along the anti-parallel merging lines poleward of the cusp extending toward the dusk side when IMF  $B_y/B_z \gg 1$ . The magnetic tension force on the newly reconnected field lines drives the plasma to move from dusk to dawn in the polar cusp region near the polar cap boundary. The field-aligned currents in the cusp region flow downward into the ionosphere. The return field-aligned currents extend into the polar cap in the center of the dayside convection cell. The field-aligned currents are closed through the Peterson currents in the ionosphere, which flow poleward from the polar cap boundary along the electric field direction.

## 1. Introduction

Magnetic reconnection, originally proposed by Dungey [1961], is the principal mechanism in solar wind-magnetosphere-ionosphere coupling process that transfer solar wind mass, momentum and energy to the magnetosphere. Field-aligned currents electrically couple the outer magnetosphere to the ionosphere. They transmit the stress applied by the reconnection from the magnetopause to the ionosphere, which drives large-scale plasma convection in the magnetosphere and ionosphere.

Polar cusp and cusp field-aligned currents are of great interest in the study of the coupling process since the solar wind plasma has direct access to low altitudes in this region. Saunders [1989] proposed a model for the origin of cusp field-aligned currents due to the dayside reconnection. In this model, the motion of newly reconnected field lines following quasi-steady reconnection at the dayside magnetopause is caused by two combined effects: the magnetic tension force on the field lines and the diverging magnetosheath flow directed radially away from the subsolar point. The newly opened field lines are pulled toward east/west direction initially in response to the IMF  $B_y$  component, and subsequently anti-sunward in the direction of magnetosheath flow, resulting in dawnward/duskward plasma convection at field line footprints near the dayside polar cap boundary. Field-aligned currents arise where the convection flow has a vorticity, which are associated with Alfvén waves that transmit the stress between magnetopause and the ionosphere [Cowley, 2000].

Although Saunders' model is for reconnection at the dayside magnetopause for southward IMF, the reconnection is not limited to southward IMF and occurs for other IMF orientations. As suggested in the anti-parallel merging model by Crooker [1979], the

merging between the IMF in arbitrary orientations and the Earth's magnetic field occurs preferentially at the magnetopause where the fields are anti-parallel. When the IMF does not have a southward component, the merging line in the model emanates from the cusps entirely on open lobe field lines in the dusk (dawn) side in the northern hemisphere for positive (negative) IMF  $B_y$  component, and vice versa in the southern hemisphere. As a consequence, there is no flux transfer from dayside closed field line to lobe open field due to the reconnection, opposite to the case for southward IMF. The polar cap convection streamlines are confined within the polar cap boundary and only transfer flux from one side of lobe to the other, the so-called lobe cell convection. For positive IMF  $B_y$  component, the anti-parallel reconnection occurs in the dusk side of the northern lobe and the magnetic tension force pulls the newly reconnected field line in the northern hemisphere toward the dawn side. The dayside polar cap convection becomes a single vortex with streamlines from dusk to dawn in the dayside northern hemisphere (Figure 5 in Crooker [1979]).

Observationally, the large-scale convection patterns in the ionosphere for northward IMF are not as well understood as those for southward IMF. Two-cell convection patterns with antisunward flow over the polar cap are consistently observed in data and predicted by models for southward IMF. However, many different convection patterns have been reported for northward IMF. Russell [1972] first proposed that sunward convection within the polar cap would be driven by reconnection between northward IMF and open field lines poleward of cusps. The plasma convection would form two reverse cells, a clockwise cell in the morning sector and a counterclockwise cell in the afternoon sector, circulating within the northern polar cap. Maezawa [1976]

confirmed this prediction using ground-based magnetic field data to show observational evidence of reverse convection cells in the polar cap. Later, four-cell convection patterns were reported, where two additional cells at lower latitudes with sunward flow on closed field lines in subauroral latitudes are present in addition to the two reverse cells in the polar cap [Burke et al., 1979; Reiff, 1982; Potemra et al., 1984; Weimer, 1995]. Adding to the controversy is the distorted two-cell patterns reported by Heppner and Maynard [1987], in which the two normal cells (observed commonly for southward IMF) are distorted in a degree based on the strength of the IMF  $B_z$  as it turns northward. Although subsequent observations have shown results that agree with either the distorted two-cell patterns [Rich et al., 1990] or reverse two-cell/four-cell patterns [Reiff and Heelis, 1994; Crowley et al., 1992; Huang et al., 2000], it has been reported that what type of the patterns will be observed depends on the relative strength of IMF  $B_y$  and  $B_z$  components [Knipp et al., 1991, 1993; McCormac et al., 1991; Lu et al. 1994]. The reverse two-cell/four-cell patterns occur for when IMF  $B_y$  is dominant ( $|B_y/B_z| < 1$ ), and the distorted two-cell patterns occur when IMF  $B_z$  ( $|B_y/B_z| < 1$ ) is dominant under northward IMF conditions.

In this paper, we report observations of plasma convection in the ionosphere and cusp field-aligned currents that can be readily explained in the anti-parallel reconnection framework. The observations of cusp field aligned current and ionosphere convection are made by the Fast Auroral Snapshot (FAST) spacecraft [Carlson et al., 1998] and from the assimilative mapping of ionospheric electrodynamics (AMIE) technique [Richmond and Kamide, 1988] during a prolonged interval when the IMF was northward and had a large positive  $B_y$  component. This interval occurred during the May 14-16, 1997 magnetic

cloud event. Using the FAST single trajectory observations to validate AMIE global convection pattern at key times and key locations, we are able to obtain with great confidence the global picture of ionosphere convection dominated by lobe reconnection. In turn, it helps us to understand the morphology and source of cusp field aligned currents.

## 2. Interplanetary Magnetic Field Observations

An overview of the origins and development of the May 12, 1997 coronal mass ejection at the Sun by SOHO and subsequent interplanetary observations of the magnetic cloud at 1 AU by Wind on May 14-16 was presented in Webb et al. [2000]. The Wind observations of interplanetary magnetic field and solar wind plasma conditions at 1 AU were also discussed in Jordanova et al. [2001]. The interplanetary shock preceding the magnetic cloud was observed by Wind at 01:15 UT on May 15, 2001, which was located at about  $190 R_E$  upstream from the Earth. The shock front arrived at the Earth's magnetosphere at 01:59 UT, as seen by Polar spacecraft (there are no FAST data available at this time). This gives a 44-minute time delay from the Wind spacecraft to Earth, which is similar to the 45 min time delay estimated from average upstream solar wind speed and the Wind location. The magnetic cloud followed about 8 hours after the shock front and lasted for about 15 hours in duration. The cloud's axial field was very strong, about 23 nT and was nearly along the +Y direction. The helical field was left-handed, resulting in a southward followed by northward magnetic field within the cloud.

Our period of interest is during the second half of the cloud when the magnetic field was northward and had a strong positive  $B_y$  component. Figure 1 shows the IMF data in GSM coordinates during the magnetic cloud passage as observed by Wind and IMP-8 spacecraft. The labels on the horizontal axis corresponds to times at Earth as the Wind data are shifted by 44 minutes and the IMP-8 data by 3 minutes to account for the lag time from the spacecraft to Earth. The bottom panel of Figure 1 shows the IMF clock angle, which is the angle of the IMF in the YZ plane. The angles of  $90^\circ$ ,  $0^\circ$  and  $-90^\circ$  correspond to due northward, horizontal, and due southward, respectively. The four short

bars are the times of successive FAST northern polar cap passes during the second half of the cloud, which we will discuss in details in this paper. For the last three passes (orbits 2891-2893), both the IMF  $B_y$  and  $B_z$  were positive and the IMF  $B_y$  was the dominant component ( $B_y \gg B_z$ ). For the first pass (orbit 2890), the IMF was slightly southward.



### 3. FAST Observations of Polar Cusp and Field-Aligned Currents

We now present the FAST observations during polar cap passes in the northern hemisphere for the three northward IMF cases. During these passes, the spacecraft trajectory is near the noon-midnight meridian. The spacecraft is near its orbital perigee moving from local noon to local midnight at altitudes  $\sim 400$  to  $600$  km.

The polar cap pass for FAST orbit 2891 occurs when the IMF just turns to slightly northward,  $26^\circ$  from the ecliptic plane, following more than one-hour nearly horizontal field. Plate 1 shows about 6 minute data near polar cusp region, including (from top to bottom) electron energy spectrogram averaged over all pitch angle, electron pitch angle spectra over energy range from  $5$  eV to  $30$  keV, ion energy spectra averaged over all pitch angle, ion pitch angle spectra over energy range from  $40$  eV to  $30$  keV, the density of field-aligned currents, and the residuals of the magnetic field component from IGRF 95 model field in local field-aligned coordinates. The labels in the bottom of Plate 1 include the universal time, spacecraft altitude in km, as well as the magnetic latitude and local time of the spacecraft footprints in the ionosphere.

The plasma data in top four panels in Plate 1 are from the ion and electron electrostatic analyzers on FAST. In the northern hemisphere,  $0^\circ$  pitch angle corresponds to downgoing, field-aligned particles and  $180^\circ$  pitch angle corresponds to upgoing plasma. The polar cusp is characterized by the localized, intense field-aligned particle precipitations. Equatorward of the cusp particle precipitations, the spacecraft is on closed field lines of the dayside magnetosphere, as evidenced by the presence of trapped high-energy ( $\sim 1$  -  $10$  keV) electrons, low energy ( $\sim 10$  eV) photoelectrons escaping from the ionosphere and double loss cones of ions at  $0^\circ$  and  $180^\circ$  pitch angles in the beginning of

the interval. The disappearance of high-energy trapped electrons occurs at the equatorward boundary of cusp precipitations. Apparently this is the dayside polar cap boundary, i.e., the boundary between open and closed field lines.

Poleward of the polar cap boundary, intense ion and electron precipitations are observed in a localized cusp region spanning  $4.8^\circ$  in magnetic latitude (from  $73.3^\circ$  at 1832:55 UT to  $78.1^\circ$  at 1834:05 UT) at 1245 magnetic local time at spacecraft footprints. The flux of cusp ions centers at keV but has a broad energy range from  $\sim 0.1$  keV to 10 keV. Within the same region, the bulk of the electrons has narrow energy centered at a few hundred eV, and the maximum energy only reaches  $\sim 1$  keV. These cusp precipitations are mainly of magnetosheath origin.

As the spacecraft moves away from the cusp region to polar cap, the ion precipitation is nearly absent but there are electron precipitations with keV energy extending to high latitudes. These electrons appear to be inverted-V precipitations produced by upward-directed parallel electric field [e.g., Block and Falthammar, 1990]. At the spacecraft altitude of  $\sim 400$  km in this pass, and we do not observe upgoing lower energy (few hundred eV) ion beams and ion conics that are also associated with upward-directed parallel electric field, such as those observed at  $\sim 4000$  km altitude by FAST [Pfaff et al., 1998]. Thus, the local acceleration region with parallel electric field is above the spacecraft altitude of  $\sim 400$  km in this pass. We can treat the magnetic field lines from spacecraft to the ionosphere below as equal-potential lines as we map the in-situ observations to the ionosphere later.

In the bottom panels of Figure 1 are the magnetic field observations and deduced field-aligned current density. The local field-aligned coordinate system is defined such

that **b** (blue trace) is field-aligned direction, **e** (green trace) points to eastward and is the cross product of **b** and radial direction **r**, **o** (red trace) is outward, and **o-e-b** forms a right-handed system. The density of field-aligned currents is calculated based on the magnetic field perturbation by assuming that they are infinite sheet currents locally normal to the magnetic meridian plane. As we will demonstrate using simultaneous observations of magnetic field and electric field, this appears to be a valid assumption. The current density  $j$  at the spacecraft altitude is the differentiation of the magnetic field cross-track component  $\delta B$  (which is mainly the east-west component  $\delta B_e$ ) with respect to the distance along the spacecraft cross-field track  $x$ , or  $j = (1/\mu_o) \cdot \{\partial(\delta B)/\partial x\}$ . The red trace is spin-average smoothed current density. The positive sign of  $j$  is for current flowing downward into the ionosphere and the negative upward away from the ionosphere.

Despite embedded fine structure currents, the overall field-aligned currents consist of a pair of large-scale currents with opposite polarity (bracketed by vertical lines) from the magnetic field and the current density profiles: a downward current corresponding to positive slope in the eastward component of the magnetic field ( $\delta B_e$ ) and an upward current corresponding to negative slope in the east-west component of the magnetic field as the spacecraft moves to higher latitude. Both the large-scale current sheets are on open field lines, poleward of the polar cap boundary. It is apparent that the downward current is coincident with the particle-entry cusp. The upward current extends to the polar cap within the region of inverted-V electron precipitations.

The subsequent two passes of polar cap (Orbits 2892 and 2893) during the interval of interest show similar features of the cusp and field-aligned currents. Plate 2 displayed about 7 minutes of data near the northern hemisphere polar cusp region for

FAST orbit 2892 in the same format as Plate 1. During this pass, the average IMF has a clock angle of  $30^\circ$  from the ecliptic plane. The polar cap boundary is observed at  $74.3^\circ$  invariant latitude at spacecraft footprint. The polar cusp, characterized by intense precipitations of both ions and electrons, occurs from  $\sim 2047:16$  to  $2048:12$  UT, spanning  $\sim 3.8^\circ$  in invariant latitude at  $\sim 1138$  magnetic local time. Poleward of the polar cusp and inside the polar cap, we again see inverted-V electron precipitations. From the magnetic field data and deduced current density, it is clear that the cusp field-aligned currents consist of a pair of current sheets: the downward flowing current sheet is coincident with the particle entry cusp ( $74.3^\circ$  to  $78.1^\circ$  ILAT), and the upward flowing current sheet extends into the region with inverted-V electron precipitations in the polar cap (above  $78.1^\circ$  ILAT), similar to what we see in the previous pass.

Plate 3 shows about 4 minutes of data near the northern hemisphere polar cusp region for FAST orbit 2893 in the same format as Plate 1. During this pass, the IMF has an average clock angle of  $11^\circ$  from the ecliptic plane. The polar cap boundary is observed at  $76.9^\circ$  ILAT at the spacecraft footprint. The particle entry cusp with intense precipitations of both ions and electrons occurs from  $\sim 2302:29$  to  $2303:25$  UT, spanning  $\sim 5.0^\circ$  in invariant latitude at  $\sim 1059$  magnetic local time. Poleward of the cusp region and inside the polar cap the inverted-V electron precipitations. Again, a pair opposite directed large-scale field-aligned currents are observed but the current density is smaller than in previous two passes. In this pass, the downward flowing current is coincident with the most intensive particle precipitations in the equatorward portion of the particle entry cusp, from  $\sim 76.9^\circ$  to  $80.4^\circ$  ILAT ( $2302:29$  to  $2303:25$  UT) at  $\sim 1107$  MLT. The upward

flowing current overlaps with the poleward edge of particle entry cusp and extended well into the polar cap with inverted-V electron precipitation (above 80.4° ILAT).

We examine next the simultaneous observations of the magnetic field and electric field in the field-aligned current region for the three passes. Plate 4 shows the east-west component of magnetic field  $\delta B_e$  (red traces) and the electric field component in the spacecraft spin plane (blue traces). The electric field component is labeled  $E\_ALONG\_V$  because the spacecraft spin axis is nearly perpendicular to the spacecraft orbit plane and the spacecraft velocity  $V_{sc}$  thus lies nearly in the spin plane. It is mainly in the north-south direction for these passes. The values of  $E\_ALONG\_V$  shown here are obtained by spin fits to the high-resolution data and are available every half spin ( $\sim 2.5$  s). The motional electric field  $V_{sc} \times B$ , although very small in the spin plane, has been removed.

In plate 4, it is evident that there is a very good correlation between the two independently measured quantities in the paired field-aligned current region. The large-scale structures of both quantities track each other very well in the field-aligned current region. A linear correlation between east-west magnetic field and north-south electric field is a consequence in the model where field-aligned currents are approximately to be infinite two-dimensional sheets and the current closure circuit is mainly in the meridian plane via Pederson currents [Smiddy et al., 1980]. Significant divergence via Hall currents in the east-west direction will result in a poor correlation between the two quantities [Sugiura et al., 1982].

#### 4. Plasma Convection in the Ionosphere

We present in this section plasma convection patterns in the polar ionosphere during the period of interest derived from the assimilative mapping of ionospheric electrodynamics (AMIE) technique. The plasma convection in the ionosphere is driven by the solar wind-magnetosphere-ionosphere coupling via field-aligned currents. Thus the convection pattern along with the knowledge of ionospheric conductivities contains a wealth of information on the global morphology and distribution of the field-aligned currents. The AMIE technique provides snapshots of global ionospheric convection patterns by combining simultaneous global ground- and space-based observations. From FAST magnetic field and electric field data we can obtain the plasma cross-track convection velocity along the spacecraft pass. With FAST observations to validate the AMIE global picture at key time and key locations, we can obtain with great confidence the information on the source and spatial extent of the field-aligned currents.

In Plates 5, 6, and 7, we compare simultaneous AMIE convection patterns and field-aligned current distributions with FAST observations along the spacecraft orbits presented in previous section. The AMIE patterns are derived based on 12-minute window of radar and satellite observations centered at key times of FAST cusp crossings (1835 UT for orbit 2891, 2050 UT for orbit 2892, 2305 UT for orbit 2893). The left panels show the AMIE convection patterns, where the dashed contours represent negative electric potentials, or clockwise plasma convection, and the solid contours represent positive potentials, or counter-clockwise plasma convection, with a contour interval of 5 kV. The plus and minus signs indicate the locations with most positive and negative potentials, respectively. The right panels show corresponding field-aligned currents

distribution at the key times, where the solid contours are for currents flowing downward into the ionosphere and the dashed contours are for currents flowing upward away from the ionosphere.

The FAST observations are overlain on the AMIE patterns along the track of spacecraft footprints in Plates 5, 6 and 7. The blue arc segments mark the polar cap boundary identified based on FAST plasma data. The blue dots along the spacecraft footprints give 5-minute tick marks, and the blue line marks the terminator at the field line footprints. In the left panels, the red vectors along the track are the equivalent  $\mathbf{E} \times \mathbf{B}$  flow velocity at the spacecraft plotted along the spacecraft ionosphere footprints. In the right panels, the red vectors are the polar projection of the transverse magnetic field perturbations along the track of spacecraft footprints. In the calculation of the plasma convection velocity at FAST, the transverse magnetic field perturbations include both the along-track and cross-track components, but the electric field data only includes along-track component ( $E_{ALONG_V}$ ), and thus, the convection flow velocity is only determined for the nearly cross-track component. Nevertheless, the cross-track flow velocity appears to be the dominant component along the FAST trajectory when comparing with the AMIE convection patterns. In Plates 5, 6 and 7, it is remarkable that the equivalent flow velocity along the track of FAST footprints is in excellent agreement with main features in the large-scale AMIE convection patterns near the polar cusp region (which corresponds to the key times the AMIE snapshots are taken). The direction of the flow velocity and the flow reversal sites at FAST match the AMIE convection pattern very well during the key time intervals.

In the left panel of Plate 5 (1835 UT for FAST orbit 2891), the total potential difference between the locations with plus and minus signs is 90 kV. The large-scale convection pattern is dominated by a negative potential, clockwise convection cell, which contains  $\sim 65$  kV in potential difference. The dominant cell is centered near  $82^\circ$  magnetic latitudes in the post-noon sector. The plasma circulation in the dominant cell is mainly confined to the polar cap. The positive potential region contains more structured convection cells with  $\sim 25$  kV of potential difference and is confined in a crescent-shaped region in the morning sector.

From the AMIE pattern of field aligned currents distribution (the right panel of Plate 5), it is apparent that the major current systems are located in the cusp region and the dayside polar cap. The currents with the largest density, namely the cusp currents, are flowing downward into the ionosphere, same as what are seen by FAST. The location of maximum current density is poleward of the FAST polar cap boundary at the dayside edge of the dominant convection cell, where the plasma convection is from dusk to dawn. The longitudinal extent of the cusp currents is about 7 hours, from 09 to 16 MLT, and centers slightly after local noon. The upward return currents are found mainly poleward of the cusp currents and extend to most of the dayside polar cap. The maximum current density for the return currents occurs near the center of the dominant convection cell.

In the next snapshot of AMIE convection pattern for FAST orbit 2892 (left panel of Plate 6), we see reduced overall convection level. The total potential difference decreases to 59 keV. The large-scale convection evolves into a two-cell pattern with two nearly balanced cells oriented nearly along the sun-earth line. The sunward cell is with negative potential and clockwise convection and the anti-sunward cell is with positive



potential and anti-clockwise convection. In the right panel of Plate 6, the field-aligned currents in the dayside show similar distribution pattern: downward cusp currents located poleward of the polar cap boundary and upward return currents extending into the polar cap. Again, the mapping between the field-aligned currents and plasma convection pattern is similar to the previous pass: the downward cusp currents is located at the dayside edge of the clockwise convection cell where the plasma moves from dusk to dawn, and the upward return currents center at the center of the convection cell.

In the convection pattern for FAST orbit 2893 (left panel of Plate 7), overall convection level is further reduced. The total potential difference decreases to 31 kV. Nevertheless, the convection pattern continues to show two cells oriented nearly along the sun-earth line. In the right panel of Plate 7, the field-aligned currents become much weaker comparing with previous two cases. In the dayside, the downward currents in AMIE pattern are confined in a very small region in the post-noon sector ( $\sim 12$  to  $14$  magnetic local time) poleward of polar cap boundary, and the upward currents are all over the rest of the polar cap. The weakening of the plasma convection and field aligned currents is also evident in the FAST data. FAST observations of weak downward currents poleward of the polar cap boundary in the cusp region and upward return currents in the polar cap (Plate 3) agree with the AMIE model. However, the longitudinal extent of the downward cusp currents in AMIE pattern does not match the FAST observation precisely. In the FAST data, the downward cusp currents are present poleward of the polar cap boundary at least one hour from local noon in the pre-noon sector.

To understand the evolution of the convection patterns during this interval, it is helpful to show the convection pattern at 1620 UT key time for FAST orbit 2890, when

the IMF was weakly southward with strong positive  $B_y$  component prior to the extended northern IMF interval (see Figure 1). Plate 8 shows a snapshot of AMIE convection pattern as well as FAST data for FAST orbit 2890 at dayside key time. Again, the plasma convection observed along the FAST track agrees very well with the AMIE pattern in the dayside. The AMIE convection pattern shows rather familiar merging cells for positive IMF  $B_y$  and southward  $B_z$ , where a round clockwise convection cell with negative potential is on the dusk side and a crescent counter-clockwise convection cell with positive potential on dawn side [e.g., Heelis, 1985; Crooker and Rich, 1993; Cowley, 2000]. The centers of both cells are near the polar cap boundary inferred from the FAST data, thus, the magnetic flux is being transferred continuously between the open field lines and closed field lines. This is a clear indication that the reconnection site is on closed field lines equatorward of the cusp even when the IMF is slightly southward with a large  $B_y$  component.

In comparison with the convection pattern in Plate 5a, we still see some plasma convection across the polar cap boundary but with much weaker strength, which appears to be the residuals of the decaying merging cells from previous southward IMF interval. The merging cells continue to decay and eventually reduce to a single cell in the midnight sector, as evident in Plates 6a and 7a. The major difference is the existence of a new clockwise convection cell that is mainly confined within the dayside polar cap when IMF turned to northward. The plasma convection within the dayside polar cap does not involve a net transfer of magnetic flux between the open and closed field line region, thus, is driven by the reconnection between the IMF and the open field lines poleward of the cusp, as described in Crooker [1979, 1988]. For the cases with very large positive

IMF By component, the anti-parallel reconnection site moves to dusk side of the northern lobe. The newly reconnected field moves mainly from dusk to dawn side due to the field tension, which drives the dusk-to-dawn plasma convection in the cusp region of the ionosphere, just poleward of the polar cap boundary. The reconnected field lines will then be swept tailward, resulting a single clockwise convection cell in the dayside northern polar cap.

Having understood the plasma convection in this reconnection-driven scenario, the observed morphology of cusp field-aligned currents fits in readily. The dayside clockwise convection cell has negative potential and the electric field points northward (or poleward), from the polar cap boundary to the center of the convection cell, in the cusp region. The field-aligned currents in the cusp region flow downward into the ionosphere, where there are velocity shears at the dayside boundary of the convection cell. They feed into the closure Peterson currents that flow poleward in the direction of electric field. Then the Peterson currents feed into the return field-aligned currents in the center of the convection vortex, which flow upward out of the ionosphere. The data also imply that the closure of the field-aligned currents mainly through the Peterson currents (Plate 4), and thus, the Hall currents close wholly within the ionosphere. This is also consistent with the fact that the cusp and the polar cap are fully illuminated by sunlight so that ionospheric conductivities are nearly uniform.

## 5. Discussion

The large-scale convection patterns observed for strongly positive IMF  $B_y$  and northward  $B_z$  ( $B_y/B_z \gg 1$ ) conditions exhibit two cells oriented nearly along the Sun-earth line. The sunward (anti-sunward) cell has negative (positive) potential with clockwise (counter-clockwise) plasma circulation. The observed instantaneous convection patterns differ in various degrees from statistically derived convection patterns. Although the sense of the plasma convection appears to be similar to that in the distorted two-cell statistical model for weakly northward IMF [Heppner and Maynard, 1987], the observed patterns in this study appear to be different in origin. In the distorted two-cell model, the normal convection cells for southward IMF were twisted and rotated to fit the observed plasma convection for northward IMF, through Heppner and Maynard [1987] did not offer explanation of underlying physical mechanisms. For positive IMF  $B_y$  condition, the afternoon clockwise convection cell was distorted into the morning cell area to form the distorted two-cell pattern. However, the convection for southward IMF transfers magnetic flux between open and closed field line regions and the normal convection cells center at the polar cap boundary. It is not discussed how the convection configuration changes related to the open-closed field line boundary during the distortion of the normal cells in Heppner and Maynard [1987]. In our study, the dayside convection cell is observed to be mainly circulating within the polar cap on open field lines. It appears to be a new cell that is developed after the IMF turns northward, rather than a distorted afternoon cell from southward IMF period. The decay of the two normal cells

when the IMF turned from southward to northward is apparent in the evolution of the convection cells.

The observed convection patterns in this study are similar to the reverse two-cell/four-cell statistical patterns with respect to their driving mechanisms but still differ in details. In the reverse two-cell/four-cell patterns, one of the reverse cells in the polar cap will grow at the expense of the other one as the strength of the IMF  $B_y$  increases. For positive IMF  $B_y$ , the negative potential cell in the morning will grow at the expense of positive potential cell in the afternoon. Under extreme conditions with strong positive  $B_y$ , the four-cell patterns may turn into the three-cell patterns, where there exists only a single negative potential cell within the polar cap, and the viscous-like cells at the lower latitudes remain the same. The negative potential viscous-like cell at dusk and the negative potential cell within the polar cap may combine into a larger negative potential cell in the afternoon sector, so that the convection pattern may appear to be unbalanced two cells nearly along the dusk-dawn meridian for strong positive  $B_y$  [Weimer, 1995]. The two cells seen in this study are oriented nearly along the Sun-earth line. The dayside cell has same characteristics as the expanded morning cell in the reverse two-cell patterns. However, we see an additional cell in the night side circulating across the polar cap boundary. This cell does not appear to be the viscous-like cell in the four-cell patterns.

Recently, a global MHD simulation by Raeder et al. [2000] reveals insight in convection dynamics of the magnetosphere during an interval of stable northward IMF  $B_z$  and negative IMF  $B_y$ . The ionospheric convection pattern from the simulation shows the very similar pattern observed in this study, with two cells oriented nearly along the sun-

earth line (Figure 7 of Raeder et al. [2000]). Note that their Figure 7 should be flipped about the noon-midnight meridian and sign of the potential in each cell should be reversed to compare with the results in this study for positive IMF  $B_y$ . In the simulation, both cells are driven by the reconnection occurring in a region of limited spatial extent near the dawn terminator where the IMF is anti-parallel to the lobe. The dayside cell is situated over the magnetic pole as lobe cell convection. Reconnected field lines drape over the dayside magnetosphere and are swept along the dusk flank. When mapping the lobe boundary from the tail to the ionosphere, the nightside cell is associated with the reconnected, overdraped field lines entering into the tail lobe through a singular entry site, where many flow lines cut through the open-closed field line boundary.

## 6. Summary

The passage of the May 14-16, 1997 magnetic cloud produced a prolonged interval with large positive IMF  $B_y$  and northward  $B_z$  conditions ( $B_y/B_z \gg 1$ ). It allows us to investigate driving mechanisms for the IMF- $B_y$  related plasma convection and cusp field-aligned currents. The data presented in this paper include in-situ observations of magnetic field, electric field, and electrons and ion fluxes from FAST spacecraft at  $\sim 300$ -600 km altitude and global convection patterns from AMIE procedure. Using the FAST single trajectory observations to validate the global convection patterns at key times and key locations, we have demonstrated that the AMIE procedure provides a reasonably good description of plasma circulations in the ionosphere.

Despite different level of convection, common features are found in the global morphology of the plasma convection during the interval of interest. When the IMF has a strongly positive  $B_y$  component under northward conditions, the direction of convection flow near the local noon is consistent with the anti-parallel merging model. We find that a single clockwise convection cell develops in the dayside northern hemisphere, mainly circulating within the polar cap on open field lines. A second cell with counterclockwise convection is located in the nightside circulating across the polar cap boundary. The observed two-cell convection pattern appears to be driven by the reconnection along the anti-parallel merging lines poleward of the cusp extending toward the dusk side when IMF  $B_y/B_z \gg 1$ . The magnetic tension force on the newly reconnected field lines drives the plasma to move from dusk to dawn in the polar cusp region near the polar cap boundary. The field-aligned currents in the cusp region flow downward into the ionosphere. The return field-aligned currents extend in to the polar cap in the center of

the convection cell. The field-aligned currents are found to close mainly through the Peterson currents in the ionosphere, which flow poleward from the polar cap boundary along the electric field direction.



#### Acknowledgements.

Guan Le thanks Carmen Liebrecht and Kristine Sigsbee for helping with FAST data analysis software. The WIND (R. P. Lepping, PI) and IMP-8 (A. Szabo, PI) key parameter data were provided by NSSDC CDDAW web. G. Lu was supported by NASA SEC Guest Investigator programs. R. J. Strangeway was supported by NASA.

## References

- Block, L. P., and C.-G. Falthammar, The role of magnetic-field-aligned electric fields in auroral acceleration, *J. Geophys. Res.*, 95, 5877, 1990.
- Carlson, C. W., R. F. Pfaff, and J. G. Watzin, The fast auroral snapshot (FAST) mission, *Geophys. Res. Lett.*, 25, 2013, 1998.
- Cowley, S. W. H., and W. J. Hughes, A definitive test of the Primdahl-Spangslev hypotheses concerning the nature of solar wind – magnetosphere interactions, *Planet. Space Sci.*, 34, 745-751, 1986.
- Cowley, S. W. H., Magnetosphere-ionosphere interactions: A tutorial review, in *Magnetospheric Current Systems*, edited by S.-I. Ohtani, R. Fujii, M. Heese, R. Lysak, p. 91, *Geophys. Mono.* 118, AGU, Washington, DC, 2000.
- Crooker, N. U., Dayside merging and cusp geometry, *J. Geophys. Res.*, 84, 951, 1979.
- Crooker, N. U., Mapping the merging potential from the magnetopause to the ionosphere through the dayside cusp, *J. Geophys. Res.*, 93, 7338, 1988.
- Crooker, N. U., and F. J. Rich, Lobe cell convection as a summer phenomenon, *J. Geophys. Res.*, 98, 13,403, 1993.
- Crowley, G., P. S. Cannon, C. G. Dozois, B. W. Reinisch and J. Buchau, Polar cap convection for Bz northward, *Geophys. Res. Lett.*, 19, 657, 1992.
- Heelis, R. A., Interplanetary magnetic field effects on high latitudes ionospheric convection, in *the Polar Cusp*, edited by J. A. Holter and A. Egeland, p. 293, D. Reidel Publishing Company, 1985.

- Huang, C.-S., D. A. Andre, G. J. Sofko, and A. V. Kustov, Super Dual Auroral Radar Network observations of ionospheric multicell convection during northward interplanetary magnetic field, *J. Geophys. Res.*, *105*, 7419, 2000.
- Jordanova, V. K., C. J. Farrugia, R. M. Throne, G. V. Khazanov, G. D. Reeves, and M. F. Thomsen, Modeling ring current proton precipitation by electromagnetic ion cyclotron waves during the May 14-16, 1997, storm, *J. Geophys. Res.*, *106*, 7, 2001.
- Knipp, D. J., et al., Ionospheric convection response to a magnetic cloud: A case for 14 January 1988, *J. Geophys. Res.*, *98*, 19273, 1993.
- Lu, G., et al., Interhemispheric asymmetry of the high-latitude ionospheric convection pattern, *J. Geophys. Res.*, *99*, 6491, 1994.
- McCormac, F. G., T. L. Killeen, and J. P. Thayer, The influence of IMF By on the high-latitude thermospheric circulation during northward IMF, *J. Geophys. Res.*, *96*, 115, 1991.
- Pfaff, R., J. Clemmons, C. Carlson, R. Ergun, J. McFadden, F. Mozer, M. Temerin, D. Klumpp, W. Peterson, E. Shelley, E. Moebius, L. Kistler, R. Strangeway, R. Elphic, and C. Cattell, Initial FAST observations of acceleration processes in the cusp, *Geophys. Res. Lett.*, *25*, 2037, 1998.
- Raeder, J., O. Vaisberg, V. Smirnov, and L. Avanov, Reconnection driven lobe convection: Interball Tail Probe observations and global simulations, *J. Atmos. Solar-Terres. Phys.*, *62*, 833, 2000.
- Reiff, P. H., Sunward convection in both polar caps, *J. Geophys. Res.*, *87*, 5976, 1982.

- Richmond, A. D., and K. Kamide, Mapping electrodynamic features of the high-latitude ionosphere from localized observations: Technique, *J. Geophys. Res.*, **93**, 5741, 1988.
- Russell, C. T., The configuration of the magnetosphere, in *Critical Problems of Magnetospheric Physics*, edited by E. R. Dyer, Jr., p. 1, National Academy of Sciences, Washington, D. C., 1972.
- Saunders, M. A., Origin of the cusp Birkeland currents, *Geophys. Res. Lett.*, **16**, 151, 1989.
- Smiddy, M., W. J. Burke, M. C. Kelly, N. A. Sافلةkos, M. S. Gussenhoven, D. A. Hardy, and F. J. Rich, Effects of high-latitude conductivity on observed convection electric fields and Birkeland currents, *J. Geophys. Res.*, **85**, 6811, 1980.
- Sugiura, M., N. C. Maynard, W. H. Farthing, J. P. Heppner, B. G. Ledley, and L. J. Cahill, Jr., Initial results on the correlation between the magnetic and electric fields observed from the DE-2 satellite in the field-aligned current regions, *Geophys. Res. Lett.*, **9**, 985, 1982.
- Webb, D. F., R. P. Lepping, L. F. urlaga, C. E. DeForest, D. E. Larson, S. F. Martin, S. P. Plunkett, and D. M. Rust, The origin and development of the May 1997 magnetic cloud, *J. Geophys. Res.*, **105**, 27,251, 2000.
- Weimer, D. R., Models of high-latitude electric potentials derived with a least error fit of spherical harmonic coefficients, *J. Geophys. Res.*, **100**, 19,595, 1995.

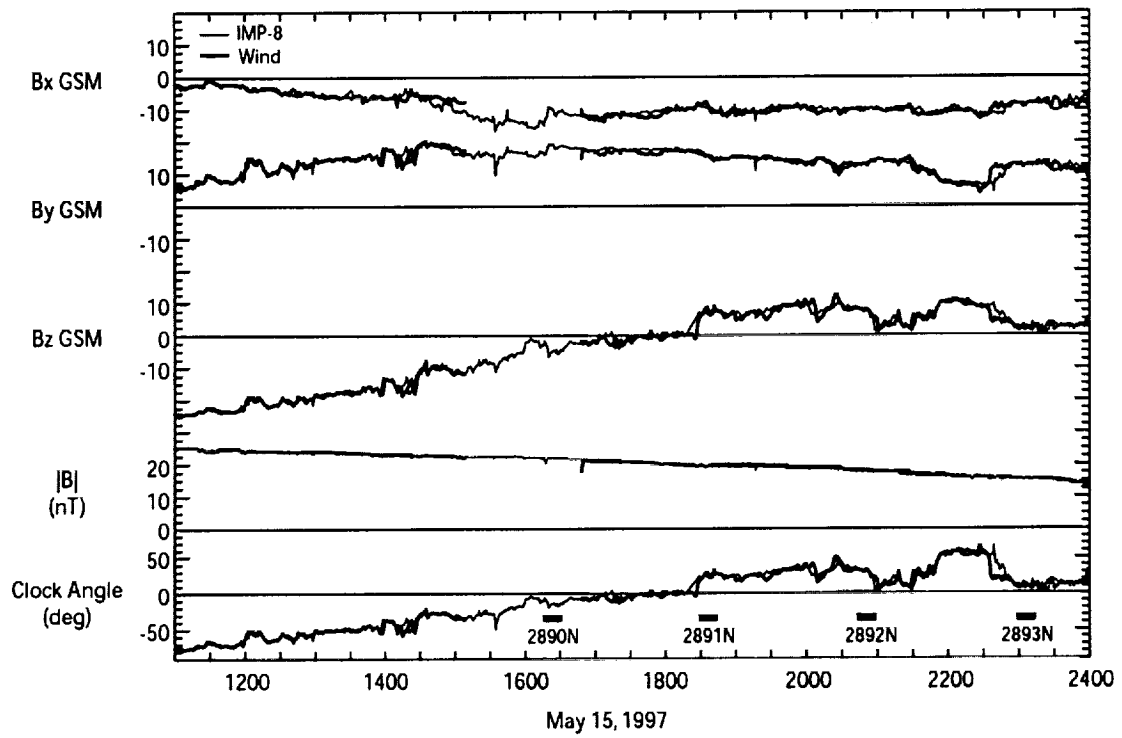


Figure 1. The interplanetary magnetic field data in GSM coordinates from Wind and IMP-8 spacecraft. . The universal time corresponds to the time at Earth as the Wind data are shifted by 44 minutes and the IMP-8 data by 3 minutes to account for the lag time from the spacecraft to Earth.

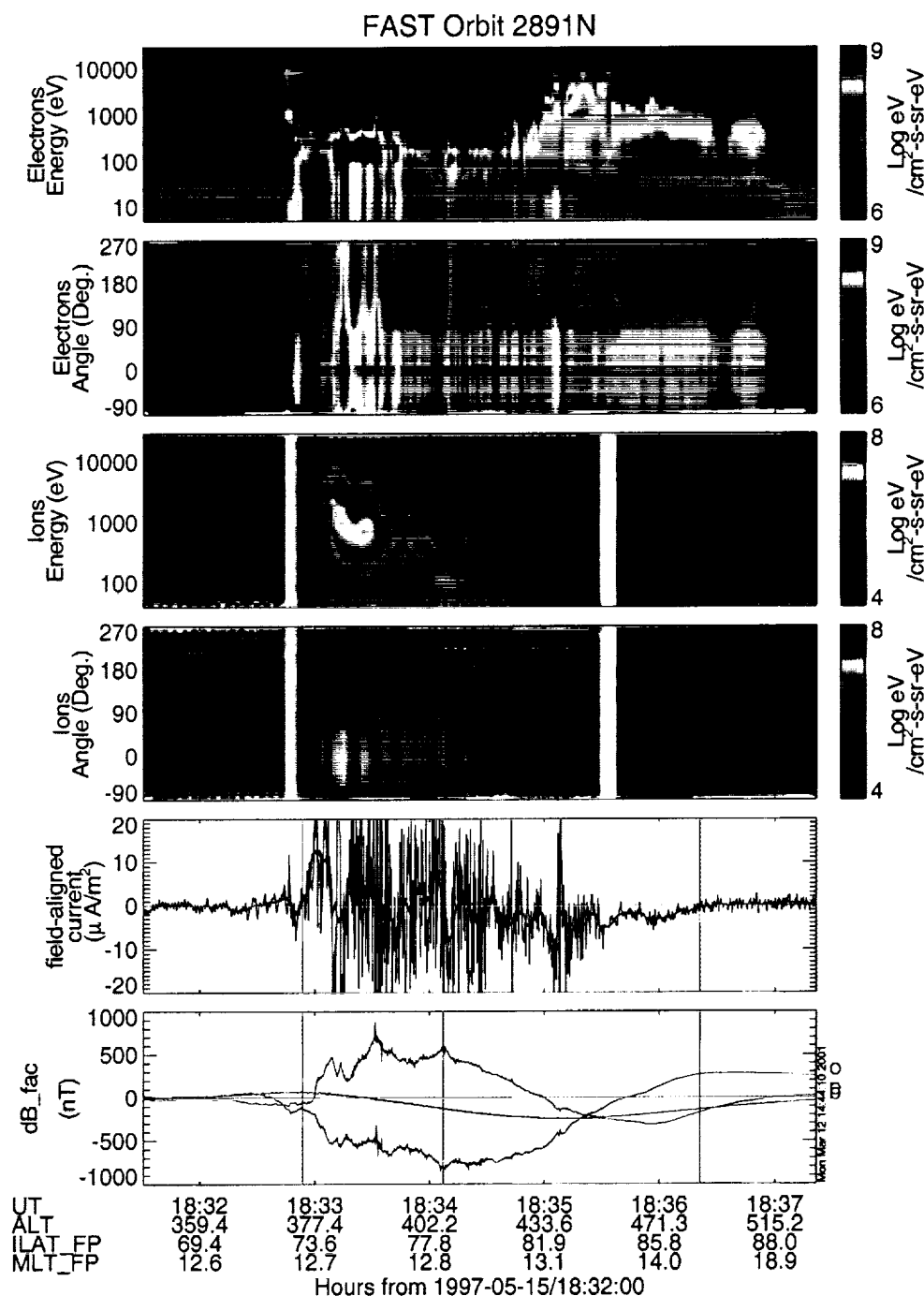


Plate 1. FAST data near polar cusp region for orbit 2891 including (from top to bottom) electron energy spectrogram averaged over all pitch angle, electron pitch angle spectra over energy range from 5 eV to 30 keV, ion energy spectra averaged over all pitch angle, ion pitch angle spectra over energy range from 40 eV to 30 keV, the density of field-aligned currents, and the residuals of the magnetic field component from IGRF 95 model field in local field-aligned coordinates.

# FAST Orbit 2892N

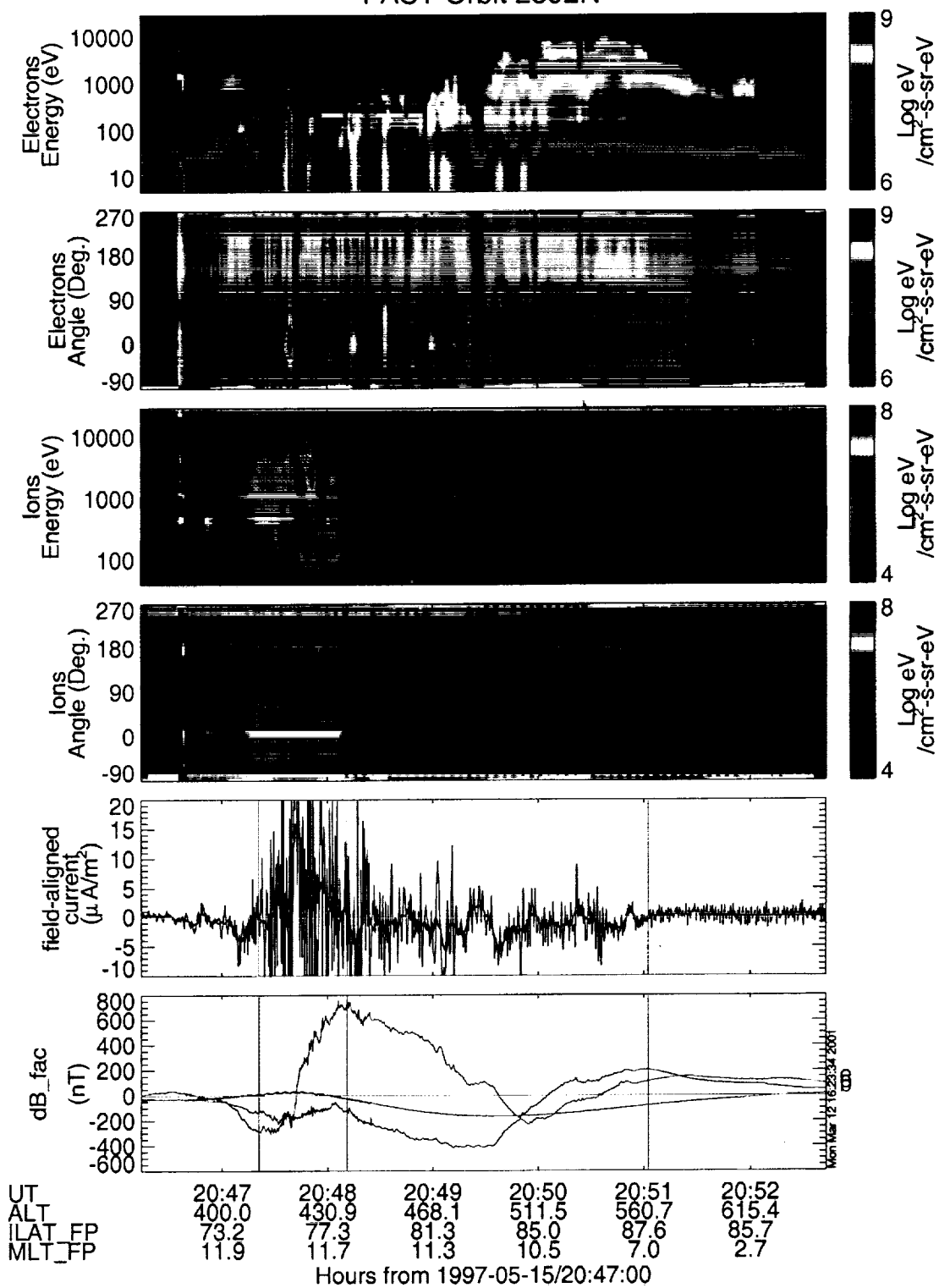


Plate 2. FAST data near polar cusp region for orbit 2892 in the same format as in Plate 1.

# FAST Orbit 2893N

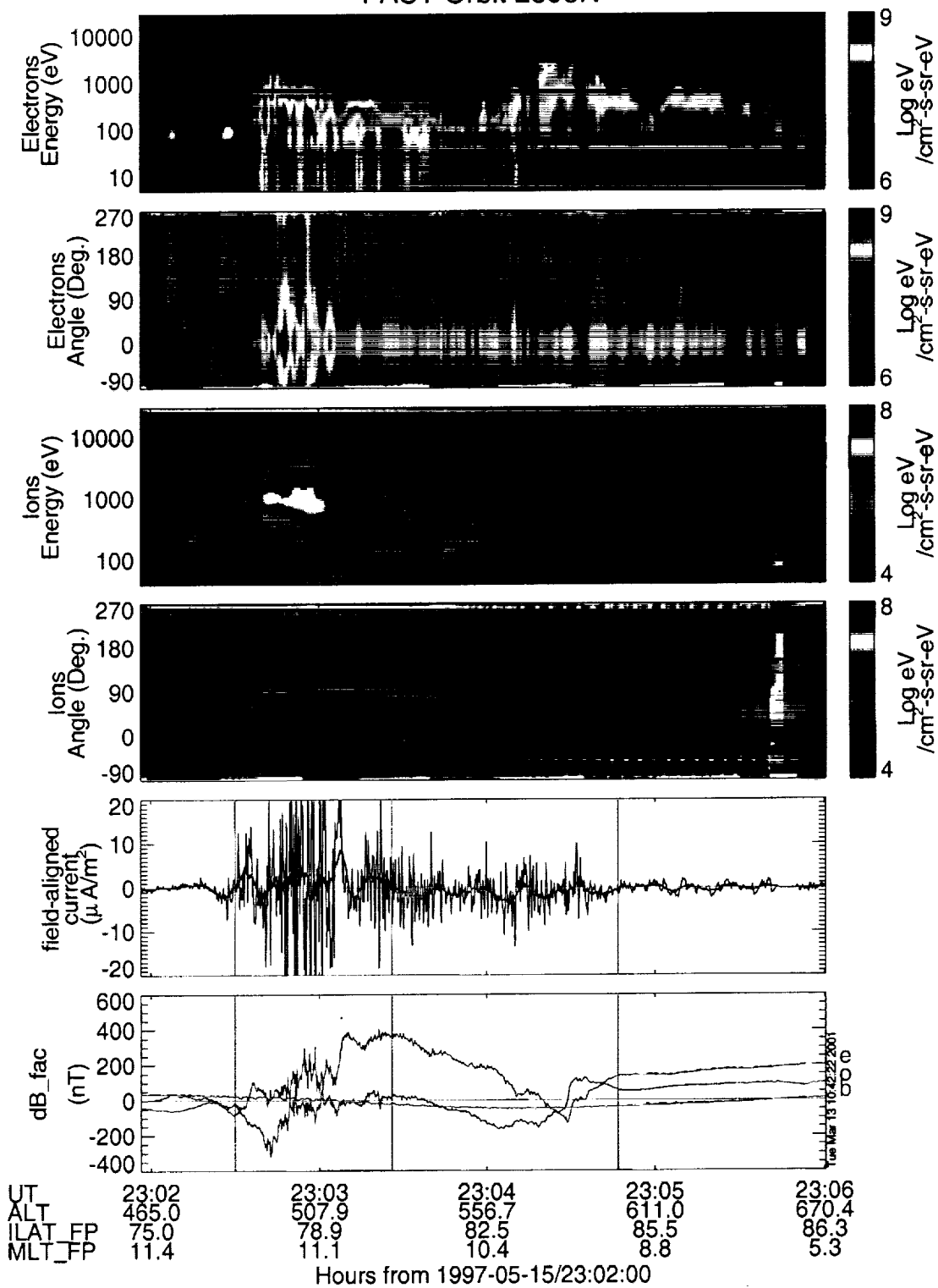


Plate 3. FAST data near polar cusp region for orbit 2893 in the same format as in Plate 3.



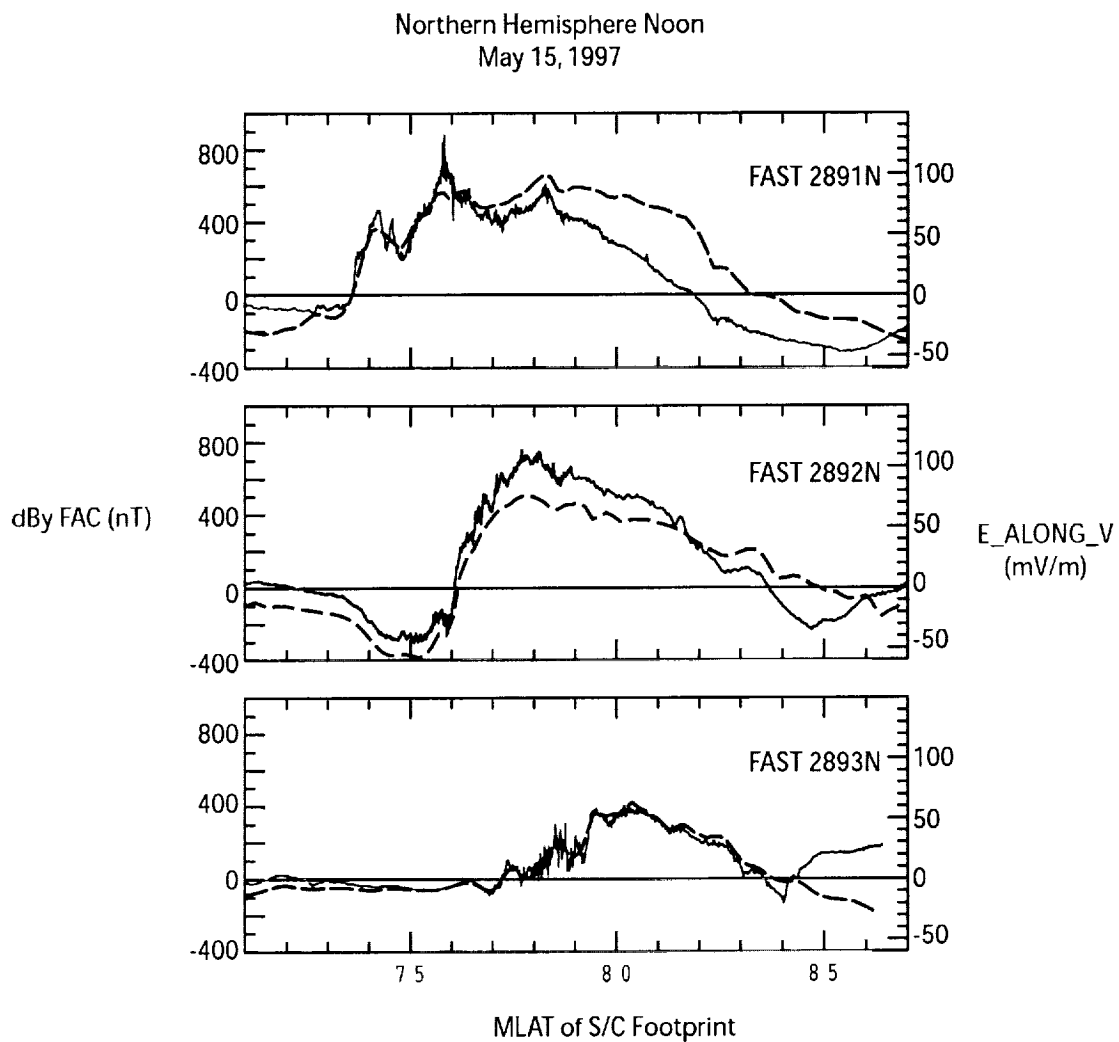
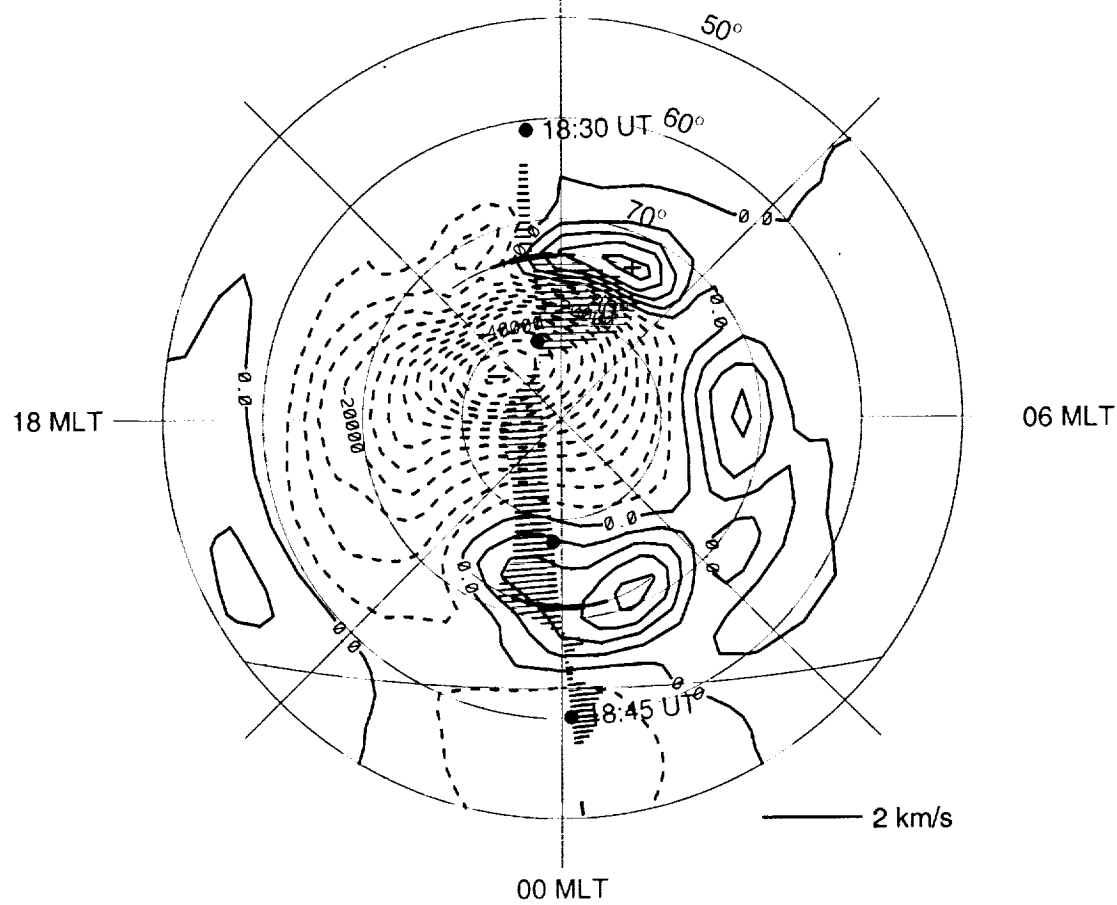


Plate 4. FAST magnetic and electric field data in the field-aligned current region. The red and blue traces are the east-west component of magnetic field  $\delta B_e$  and the electric field component in the spacecraft spin plane, respectively.

1997 MAY 15 18:35 UT

12 MLT



—— In Eclipse

1997-05-15 18:30 - 18:45

Plate 5a.

FAST Footprints: Orbit 2891 - North  
1997 MAY 15 18:35 UT

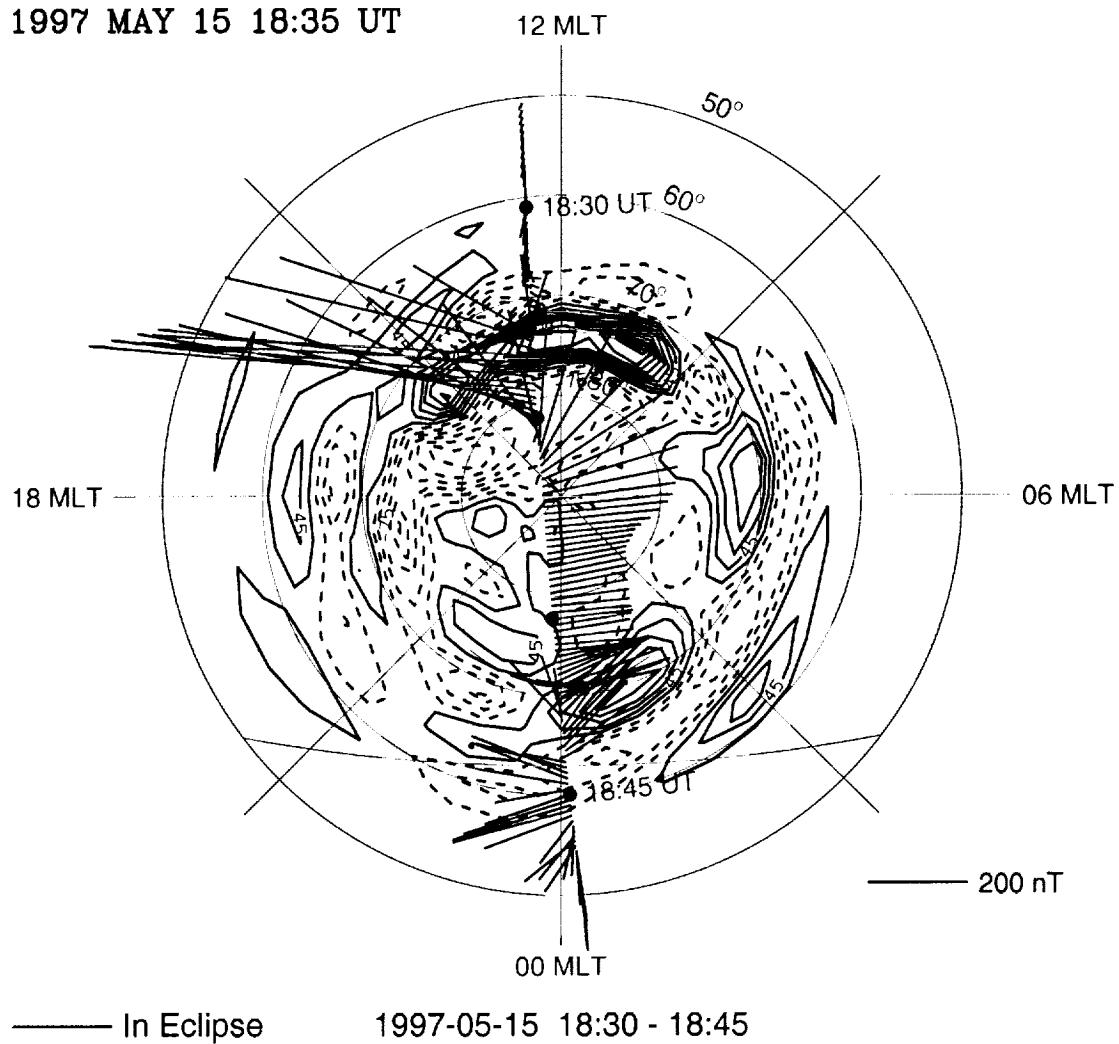


Plate 5b.

Plate 5. The FAST observations are overlain on the AMIE patterns along the track of spacecraft footprints for orbit 2891. The IMF was northward with a large positive  $B_y$  component during this interval.

FAST Footprints: Orbit 2892 - North  
 1997 MAY 15 20:50 UT

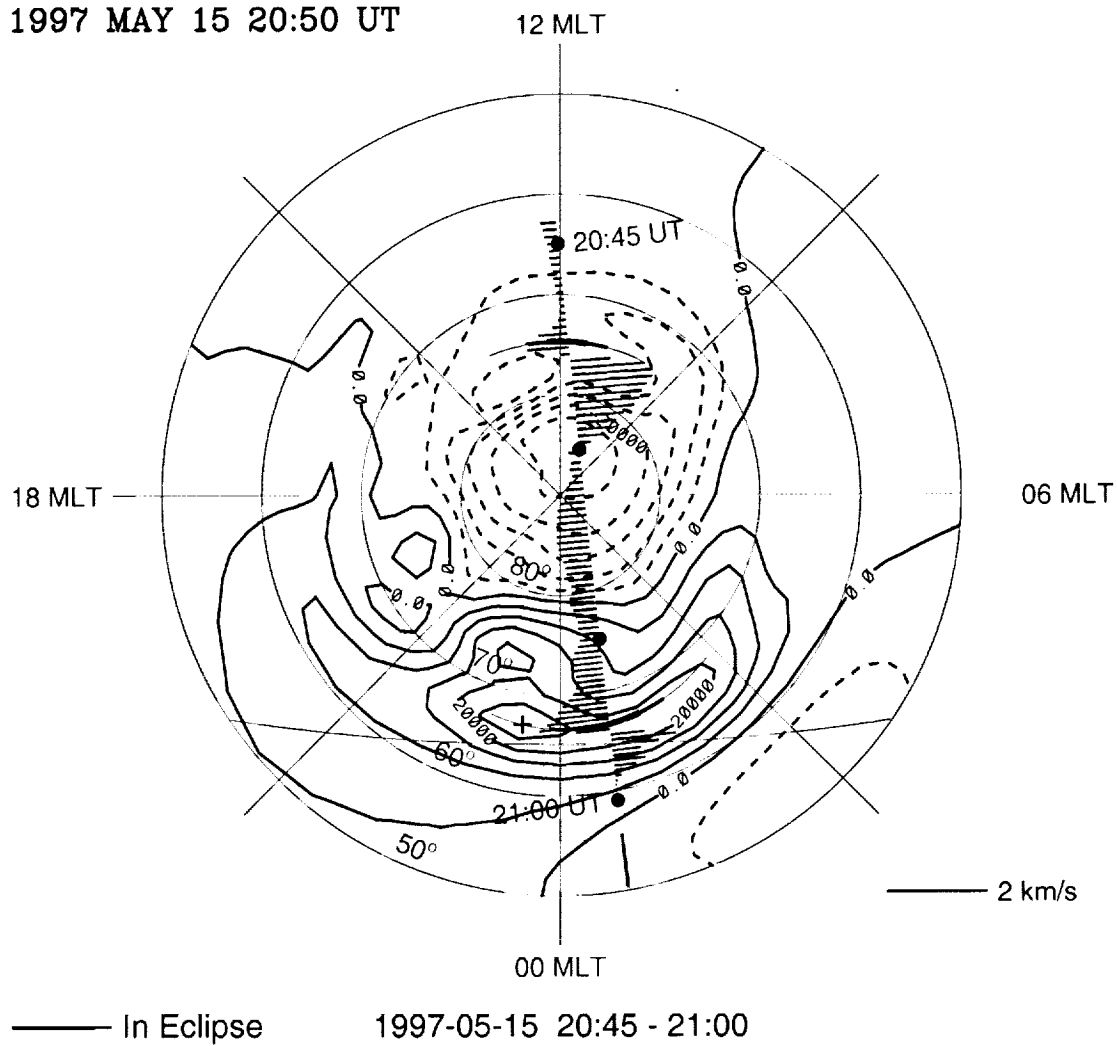


Plate 6a.

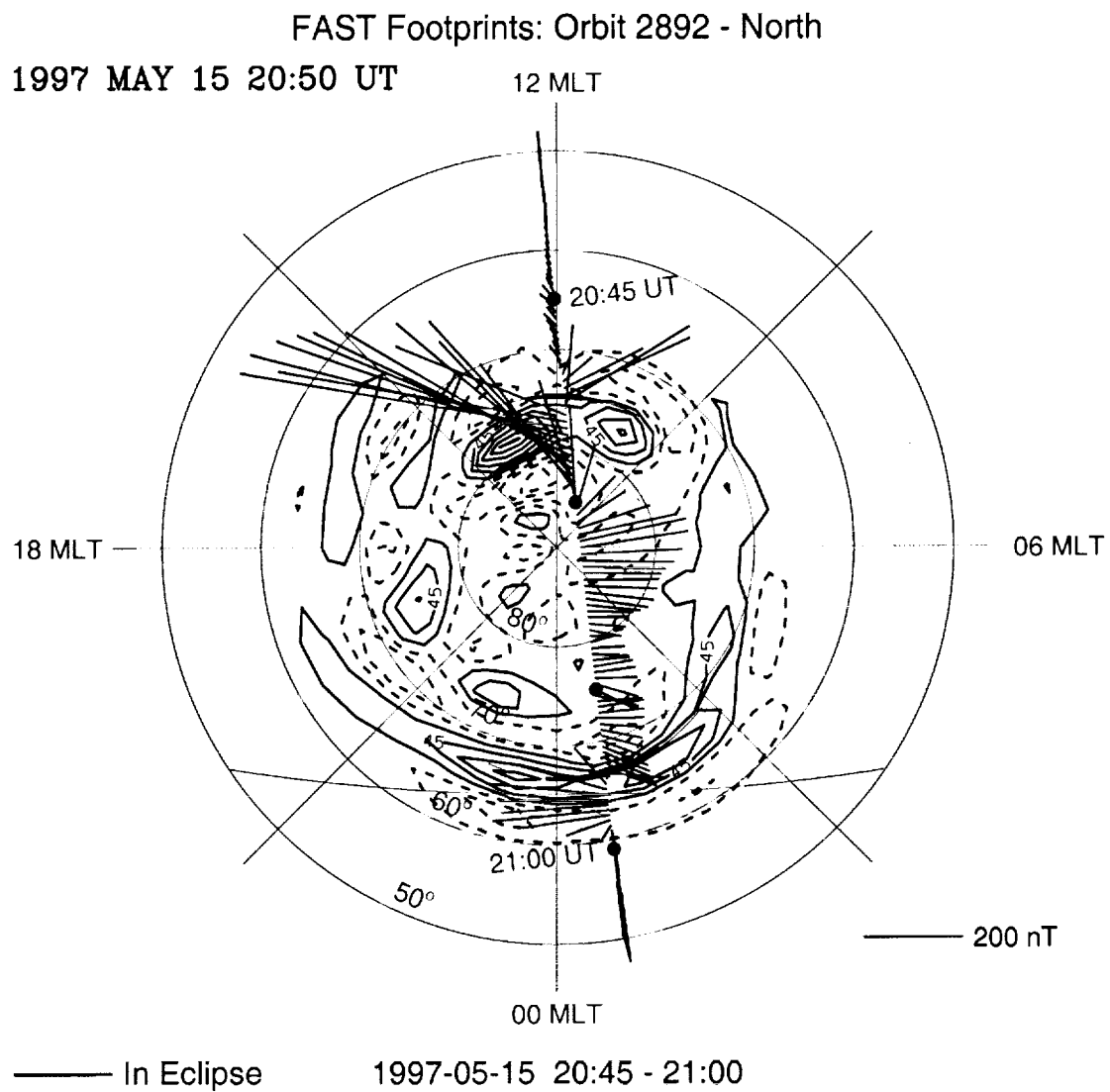
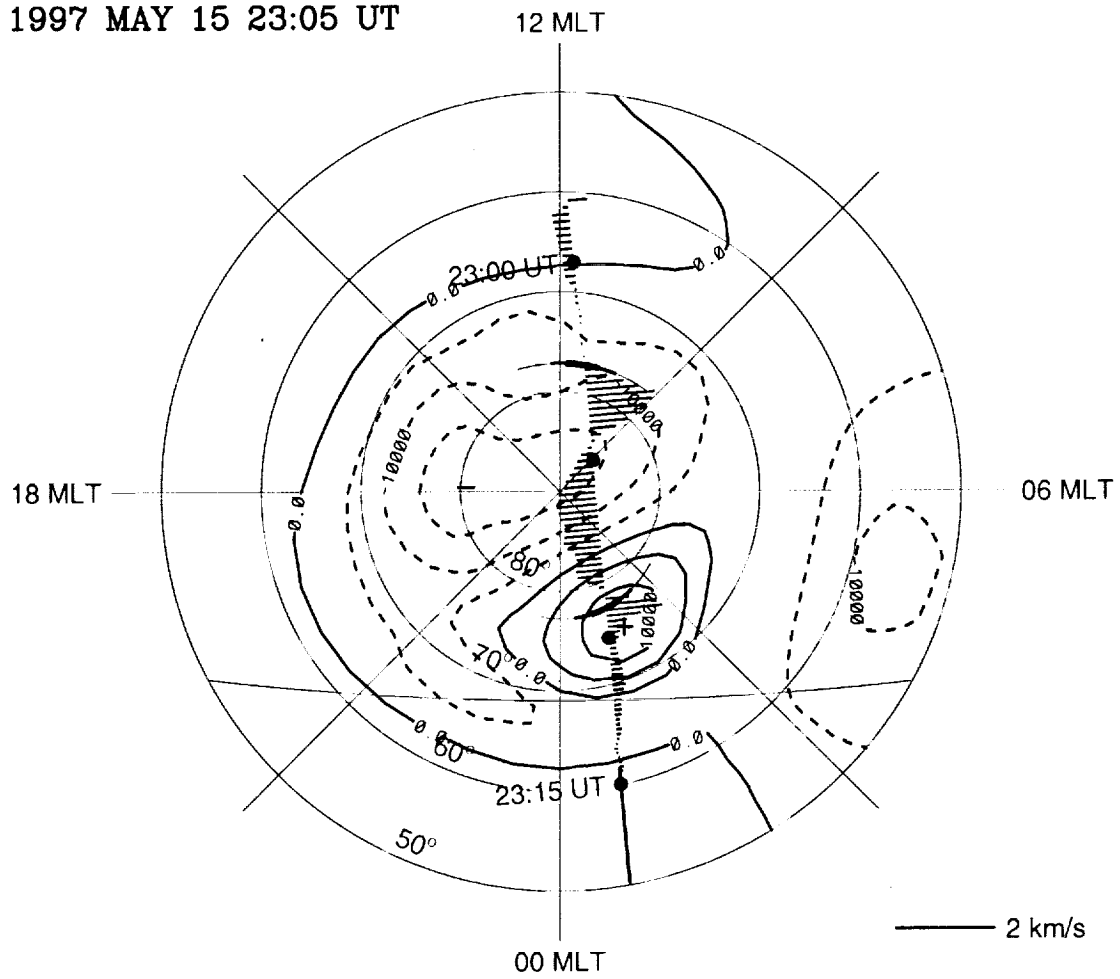


Plate 6b.

Plate 6. The FAST observations are overlain on the AMIE patterns along the track of spacecraft footprints for orbit 2892. The IMF was northward with a large positive  $B_y$  component during this interval.

# FAST Footprints: Orbit 2893 - North

1997 MAY 15 23:05 UT



— In Eclipse

1997-05-15 23:00 - 23:15

Plate 7a.

FAST Footprints: Orbit 2893 - North  
1997 MAY 15 23:05 UT

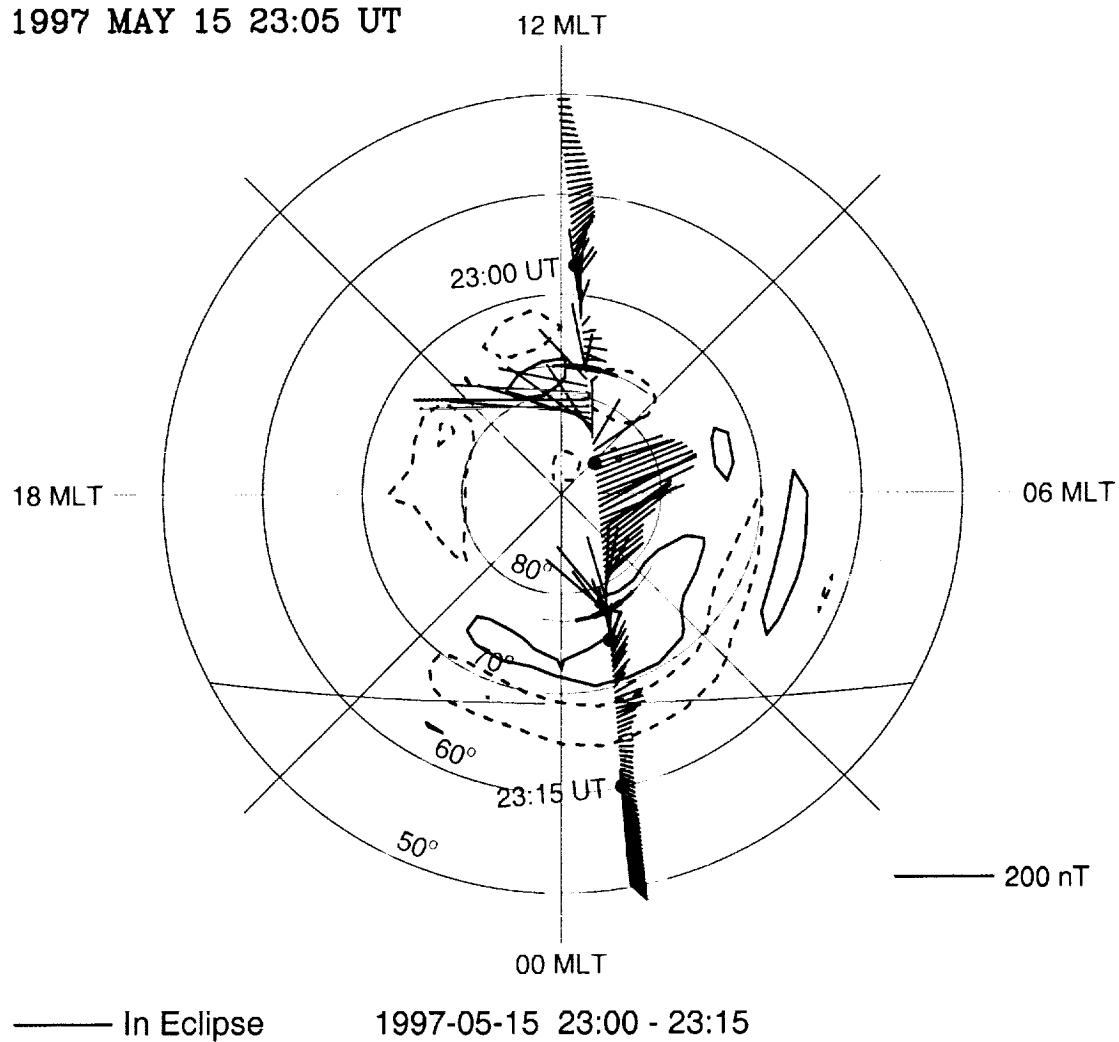


Plate 7b.

Plate 7. The FAST observations are overlain on the AMIE patterns along the track of spacecraft footprints for orbit 2893. The IMF was northward with a large positive  $B_y$  component during this interval.

FAST Footprints: Orbit 2890 - North  
1997 MAY 15 16:20 UT

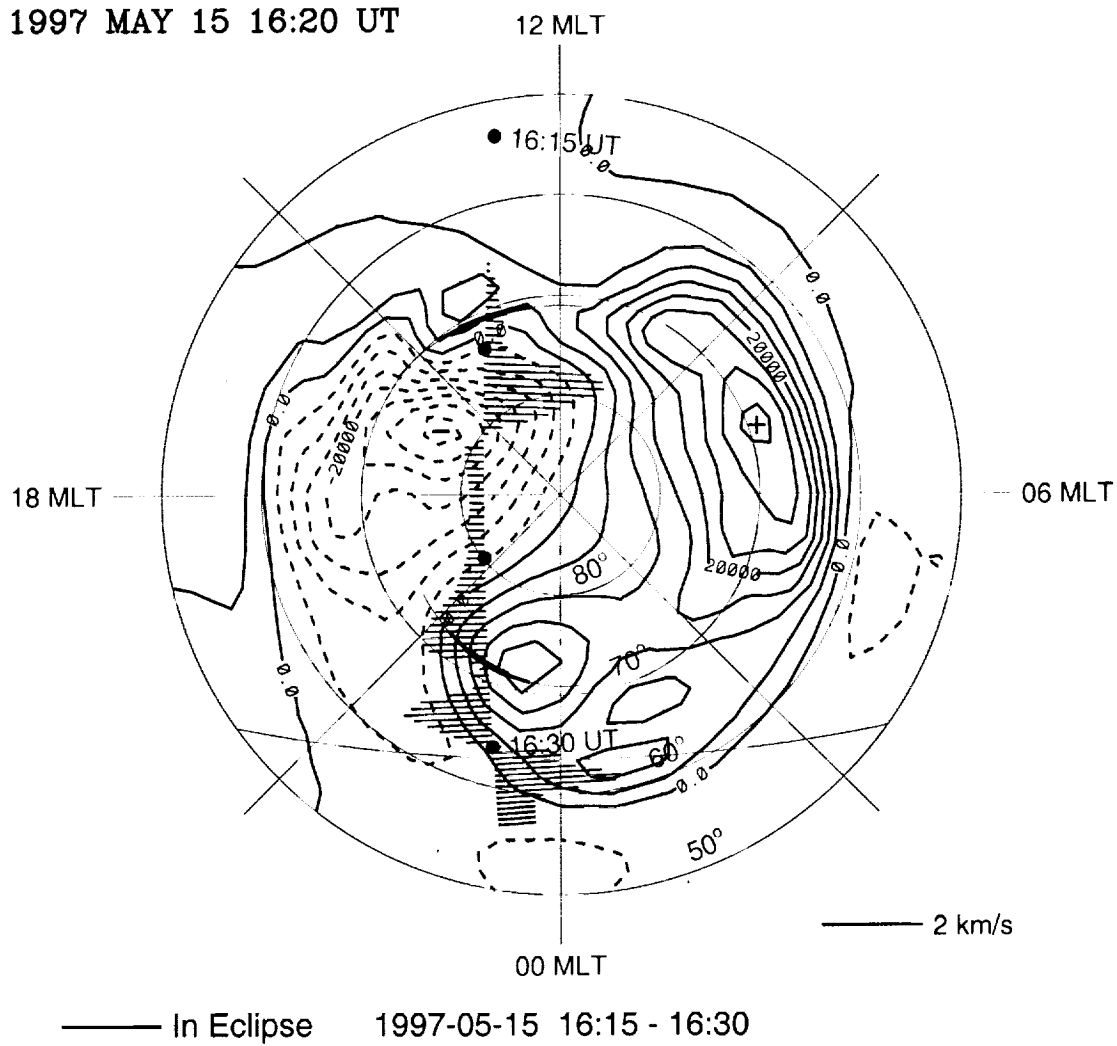


Plate 8.

Plate 8. The FAST observations of plasma convection velocity are overlain on the AMIE convection pattern along the track of spacecraft footprints for orbit 2890. The IMF was slightly southward with a large positive  $B_y$  component during this interval.